Int. J. Electrochem. Sci., 15 **(2020)** 6938 – 6954, doi: 10.20964/2020.07.79

International Journal of ELECTROCHEMICAL SCIENCE
www.electrochemsci.org

Preparation and Characterization of Polyamide6/Organic Clay Nanocomposite as protective coating for Carbon Steel

Layla A. Al Juhaiman[*], *Alanood A. Aljaghwani*, *Waffa K. Mekhamer*

Chemistry Department, King Saud University, Riyadh , Saudi Arabia
[*]E-mail: ljuhiman@ksu.edu.sa

Received: 30 March 2019 / *Accepted:* 16 February 2020 / *Published:* 10 June 2020

In this work Polyamide/organic clay nanocomposite (PCN) was successfully prepared. The raw clay was collected from Khulays area north of Jeddah in Saudi Arabia. After grinding, it was washed with water, thereafter it was saturated with 0.5M NaCl solution to obtain the sodium clay (NaC). To obtain the organoclay (OC), the NaC was modified with Cetylpyridinium chloride (CPC). Polyamide6/organoclay nanocomposites (PA6/OC NCs) were prepared at 1,2,3,4 and 5 wt% of OC. The PA6/OC nanocomposites were characterized using Fourier transform infrared spectroscopy (FTIR), X-ray Diffraction (XRD), Scanning electron microscope (SEM) as well as transmission electron microscope (TEM). The FT-IR spectra of OC show the appearance of new bands of the constituents of CPC which gives an evidence for the presence of the organic component CPC in the OC structure. The XRD results for OC showed a shift in d_{001} spacing from 10.93˚A for NaC to 20.63˚A for OC. The XRD results for PA6/OC nanocomposites showed the loss of the clay crystalline structure at the low clay loading of 1-3 wt%. From TEM results, the PA6/OC nanocomposites at 1, 2, and 3wt% of OC showed exfoliated structures while the 4 and 5wt% showed small portion of intercalated structure. The SEM results for the OC and PA6/OC showed a good homogeneous mixture in the PA6/OC nanocomposites. The anticorrosive properties of PA6/OC nanocomposites coatings on C-Steel were investigated using electrochemical impedance spectroscopy (EIS) and Potentiodynamic polarization in 3.5 wt% NaCl electrolyte. Results showed that the PA6/OC nanocomposite coatings have better corrosion protection of C-Steel than pure PA6. The PA6/OC nanocomposite coatings containing 5wt% of the OC exhibited the best corrosion protection which reached about 75%.

Keywords: Polyamide6; Organic clay; Nanocomposite; XRD; EIS; Potentiodynamic polarization

1. INTRODUCTION

Toyota research group is considered as one of the earliest research group to have used nanoparticles to produce a polyamide 6/MMT nanocomposite. They used it commercially by adding small loading of MMT (4.2 wt%) to PA6[1, 2]. The PA6/MMT nanocomposite showed an increase in

tensile strength, modulus, heat distortion temperature and a decrease in the combustion heat release rate [1, 2]. It was reported that the benefits of adding the nanoscale material to the polymer matrix are increase in strength, hardness, scratch resistance and corrosion protection [3,4,5]. Polymer has been used as a coating to protect metals against corrosive species but polymeric coating doesn't give full protection to the metal surface due to the defect that may occur. Adding a reinforcement to the polymer with plate-like structures increases the length of diffusion pathways for corrosive species to reach the metal surface and decrease the permeability of the coating [4]. Nanocomposites are regarded as a new class of composites, where the fillers are in the nano meter scale at least in one dimension. The properties of polymer clay nanocomposites depend on the dispersion of polymer into the clay layers and the interaction between the polymer chains and the clay surface.

Clay minerals are naturally abundant, environmentally friendly material which has a huge cation exchange capacity. Clay has particle size less than 2μm and about 1 nm layer thickness and certain plasticity when mixed with a suitable liquid, like water [2, 6]. For the preparation of Polymer-Clay nanocomposites (PCN), Smectite is regarded as the most commonly used clay minerals. Smectite belongs to the 2:1 phyllosilicates family. The crystal structure of Smectite is made up of an octahedral sheet of alumina sandwiched between two tetrahedral sheets of silica [7, 8]. Surface modification of clay minerals has attracted a lot of attention because they obtained products that exhibit properties suitable for many applications in material science, pharmaceutical applications and environmental engineering [2, 8, 9]. For the clay to exfoliate and intercalate with a polymer, the hydrophilic surface of clay needs to be modified to a hydrophobic surface to match the hydrophobicity nature of many polymers. It is common to convert the hydrophilic nature of clay to organophilic nature via a cation exchange reaction with a surfactant which contains organic cations such as alkyl ammonium or phosphonium cations that contain different substituents, one of them must be alkyl chain of 12 carbon atoms at least which will cause an increase in the interlayer distance of clay [8, 9]. The gap between the clay layers is known as the gallery or d_{001} spacing which varies depending on the size of the intercalated organic cations. The inter layer distance is affected by the alkyl chain length of the surfactant, the charge density of the clay and the manner at which the alkyl tail of the surfactant molecules organize themselves in the organoclay.

Generally, there are four methods for the preparation of PCN which include solution intercalation (solution blending), in-situ intercalative polymerization, in-situ template synthesis and melt intercalation [8]. Polymer clay nanocomposite structures are classified based on the exfoliation and intercalation levels of the polymer chains into the clay galleries which can be affected by several parameters such as clay nature, organic modifier, preparation methods and polymer matrix. In the present study, we used solution intercalation (solution blending) method. The exfoliated polymer/clay nanocomposites are usually desirable to improve the PCN properties due to the large aspect ratio and homogenous dispersion of clay and large interfacial area between polymer and clay [5, 6, 9].

Polyamide 6 (PA6) is a thermoplastic polymer prepared via condensation polymerization. Due to its mechanical and thermal properties, it has been widely used in industrial applications such as films, fibres and textiles. However, these advantages have some limitations such as moisture absorption, poor dimensional stability and low impact strength [10-14]. The use of PA6 in Toyota research group inspired us to use PA6 to prepare polymer clay nanocomposite using modified local clay. Therefore, the aim of

this work is the modification of raw Khulays clay in order to be compatible with the polymer. The first stage is washing the clay with NaCl then with the surfactant Cetylpyridinium chloride (CPC) to obtain the Organo Clay (OC). The preparation of PA6/organo clay nanocomposite (PA6/OCNs) was accomplished using solution blending method. The characterization of PA6/OC NCs was performed using FT-IR, XRD, SEM and TEM. In addition, we aim to study the anticorrosive properties of PA6/OC NCs coatings on C-Steel electrodes in NaCl solution by electrochemical methods such as electrochemical impedance spectroscopy and Potentiodynamic polarization.

2. EXPERIMENTAL

2.1. Chemicals and reagents

The Raw Clay (RC) was collected from Khulays region western side of Jeddah, Saudi Arabia and ground in our laboratory. The chemical composition and XRD of raw clay have been reported by previous studies [15, 16]. Sodium Chloride (AR grade) from Win lab Company was used to prepare 3.5 wt% NaCl solution as the electrolyte and corrosive environment to simulate sea water conditions. Cetylpyridinium chloride (CPC) was purchased from BDH Chemicals Ltd Pools, England having a molecular weight of 358.01 g/mol, cationic activity 98%, melting point82 to 84°C. CPC was chosen as it contains 16 methyl groups. Polyamide 6 (PA6) was purchased from Sigma-Aldrich Company, having density of 1.084 g/ml at 25°C. The solvent used to dissolve PA6 was m-cresol. It was purchased from TECNO Pharm chem Hyrana, India. The C-Steel is a commercial rod of steel (grade 1046) with 98.46% iron. They were purchased from ODS company in Germany. The chemical composition has been presented earlier [16].

2.2. Apparatus

The coating thickness of C steel samples was done using a coating thickness gauge from electrometer 465. A Perkin Elmer FT-IR system Spectrum BX 100 was used to record the FT-IR spectra of the samples. X-ray Diffraction analysis (XRD) was recorded using a Bruker (D8 ADVANCED). The Scanning Electron Microscopy (SEM) was performed on JEOL JSM7610F LTD while Transmission Electron Microscopy (TEM) was performed on JEM-1400. All of the electrochemical methods used in this study were achieved using a potentiostat\galvanostat from ACM Instruments (UK).

2.3. Preparation of PCN

The method of washing, separation, saturation with NaCl and modification of Khulays clay with the surfactant has been presented in a previous study [15,16]. Several solvents have been tested to dissolve the polyamide 6: Tetra hydro Furan (THF), Dimethyl formamide (DMF) and Cyclohexanone, but they did not dissolve PA6. Although formic acid is an excellent solvent of PA6 in many applications, the corrosive effect of formic acid on C-Steel restricted its use in this study. Thus, m-cresol was chosen

as a solvent for PA6 to study the protective effect of PA6 and PA6/OC NCs on C-Steel in 3.5% NaCl medium. The organic clay (OC) was prepared by a cation exchange reaction between the sodium cations of NaC and the surfactant cetylpyridinium chloride cations. PA6/OC NCs films were prepared via solvent casting method at different masses of OC (0, 1, 2, 3, 4 and 5 wt%). In a 25 ml flask, the required mass of the Organic clay was added to 10 ml of m-cresol and stirred magnetically at room temperature overnight, then 0.6 g of PA6 was added. The mixture was stirred magnetically overnight to allow the polymer to dissolve and intercalate with OC, then it was sonicated for 20 min. Thereafter, the mixture was casted on glass slides with a dimension of 50 × 15 mm. The slides were left overnight to evaporate the m-cresol at room temperature, then the films were removed from the glass slide and used for the characterization methods.

2.4. Preparation of Coatings

Carbon Steel (C-Steel) rod samples were used as the working electrodes. The cross-sectional area of each rod is 6.3 cm^2. The surface of the working electrode was polished with abrasive papers of different grades (80-220-800). The C-Steel rods were washed thoroughly with distilled water then cleaned for 2 min in acetone in an ultrasonic bath. The PA6 and PA6/OC solutions were casted on the C-Steel rods followed by drying under vacuum to give coating thickness of ≈ 15±5 μm, as measured by coating thickness gauge (from electrometer 465).

2.5. Characterization experiments

Fourier transform infrared spectroscopy (FT-IR) was performed at a wavelength range of 400 – 4400 cm^{-1}. For an Infrared analysis, the KBr pressed disc technique is regularly used.

X-ray Diffraction analysis (XRD) was performed at room temperature. The XRD patterns were recorded in the range of 3° - 50° at a wavelength of (λ=1.54060 A°), at diffraction angle 2θ with a scanning rate of 0.3°/s using radiation operator at 40 kV and 40 mA.

Scanning Electron Microscopy (SEM) was performed to observe the morphology of the OC. The samples were mounted on carbon and the surface was coated with gold.

Transmission Electron Microscopy (TEM) was performed to observe the morphology of the OC and PA6/OC NCs films. The PA6/OC films were embedded in an epoxy resin and cured overnight at 55°C. Then, they were dissected with a microtome to produce ~80-100 nm thick sections. Ultrathin sections were prepared with a diamond knife, and the final images were captured by placing the samples on carbon-coated 200 mesh Cu grids. OC was dispersed in distilled water, then a droplet from the suspension was put on para film and thereafter moved onto the grid and left to dry at room temperature.

2.6. Electrochemical experiments

Three electrochemical techniques were used in this study. These techniques are operated as a sequence that started with open circuit potential (OCP) for 60 minutes to achieve equilibrium. The

variation of steady state potentials (E_{ss}) with time was recorded with respect to SCE. When a steady potential was established, the impedance measurements will start, followed by Potentiodynamic polarization. The experiments were repeated at least three times to ensure reproducibility and statistical significance and the average results were reported. A three-electrode cell was used: C-Steel rod as the working electrode with an exposed area of 6.3 cm^2, a saturated calomel electrode (SCE) as the reference electrode and a Platinum auxiliary electrode. All tests were performed in a corrosive medium (3.5 wt% aqueous NaCl). The electrolyte's temperature was maintained at 30 ±1ºC using a water bath. The open circuit potential (OCP) at the equilibrium state of the system was recorded as the corrosion potential (E_{ss} in volts vs. SCE). Impedance measurements were performed after OCP. The Nyquist diagram shows the relationship between Z'-real impedance (x-axis) and Z"-imaginary impedance (y –axis) over a wide range of frequency values (30×10^3 to 0.01Hz). The Impedance (Z) depends on many parameters: the solution resistance (R_{sol}), the charge transfer resistance (Rc), the capacitance of the electrical double layer (C_{dl}), and the frequency of the AC signal (ω). Potentiodynamic polarization was obtained by scanning the potential from 250 mV below the E_{corr} value to 250 mV above the E_{corr} value at a scan rate of 60 mV/min. The corrosion current density (i_{corr}) was determined by superimposing a straight line along the linear portion of the cathodic or anodic curve and extrapolating it through E_{corr}

3. RESULTS AND DISCUSSION

3.1 Characterization experiments

3.1.1 Fourier transform infrared spectroscopy (FT-IR)

Fourier transform infrared spectroscopy technique is considered as one of the oldest and most common technique that has many advantages such as: ease of use, low cost and fast where the spectrum can be obtained in a few minutes. **Fig. 1** shows the infrared spectrum of KBr thin discs prepared from the RC, NaC, OC and CPC. The percent transmittance of FT-IR spectrum of the unmodified and modified clay samples are shown together. The FT-IR spectra of the RC and NaC show broad bands at 3625 cm^{-1} which are related to the stretching vibration of –OH group coordinated to Al-Al. The bands that appeared at 3433 and 1642 cm^{-1} are due to the presence of absorbed water. At 1035 cm^{-1}, a broad band appeared for Si-O stretching vibration of layered silicate. At 528 and 466 cm^{-1}, broad weak bands related to Al-O-Si, Si-O-Si, and Si-O deformations are shown. For NaC, -OH stretching band shifted to 3697 cm^{-1}. The absorbed water peaks appeared at 3624 and 1638 cm^{-1}. For the Si-O, the broad band appeared at 1032 cm^{-1} while the bands for Al-O-Si, Si-O-Si, and Si-O deformations appeared at 529 and 467 cm^{-1}[17].

The FT-IR spectra of OC shows the appearance of strong bands at 3063 cm^{-1} (for =CH in the aromatic ring in CPC), 2920, 2851cm^{-1} (for the asymmetric and symmetric stretching vibration of C-H in the alkyl chains in CPC, respectively) and 1491 cm^{-1} (for the C=N in the CPC). These bands were shifted toward higher frequencies compared to the CPC spectra, which gives an evidence for the presence of the organic component CPC in the OC as demonstrated by other studies [12, 13, 17, 18]. The role of

the alkyl ammonium cations in the organo silicates is to improve the wetting characteristics of the polymer and to lower the surface energy of the inorganic clay [19]. The choice of CPC by many researchers was because it contains alkyl chains of more than 12 carbon atoms which will cause an increase in the interlayer spacing of clay [4, 6, 14, 15].

The FT-IR spectra for pure PA6 and PA6/OC NCs are shown in **Fig. 2** For pure PA6, there are two bands related to the symmetric and asymmetric stretching of the $–CH_2$ sequence at 2933 and 2860 cm^{-1} associated with a band at 697 cm^{-1} for the vibrations of $–CH_2$ groups in the polymer chain. At 3297 cm^{-1}, a strong band appeared which is related to N-H. The C=O in amide I band appeared at 1639 cm^{-1} and the bands for the combination of N-H and C-N in amide II stretching appeared at 1550 cm^{-1}[20]. For the PA6/OC NCs, the same bands appeared at the same frequencies compared to pure PA6 except for a new band that appeared at 1033 cm^{-1} which gives an indication of the presence of Si-O from OC. On increasing the OC content, the bands were shifted slightly to lower wavenumbers in PA6/OC nanocomposites. These shifts may be attributed to the dispersion of OC in the PA6 matrix [3,15].

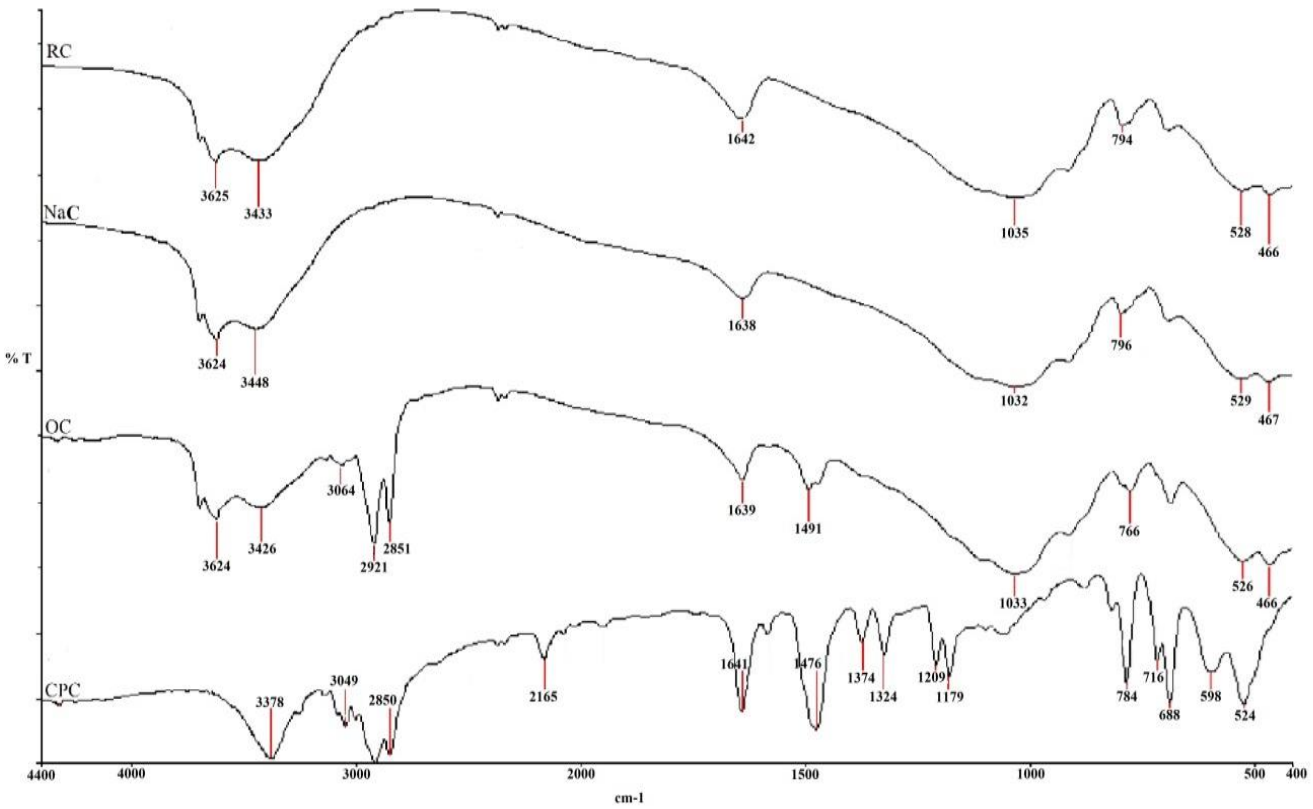

Figure 1. FT-IR spectra of RC, NaC, OC and CPC.

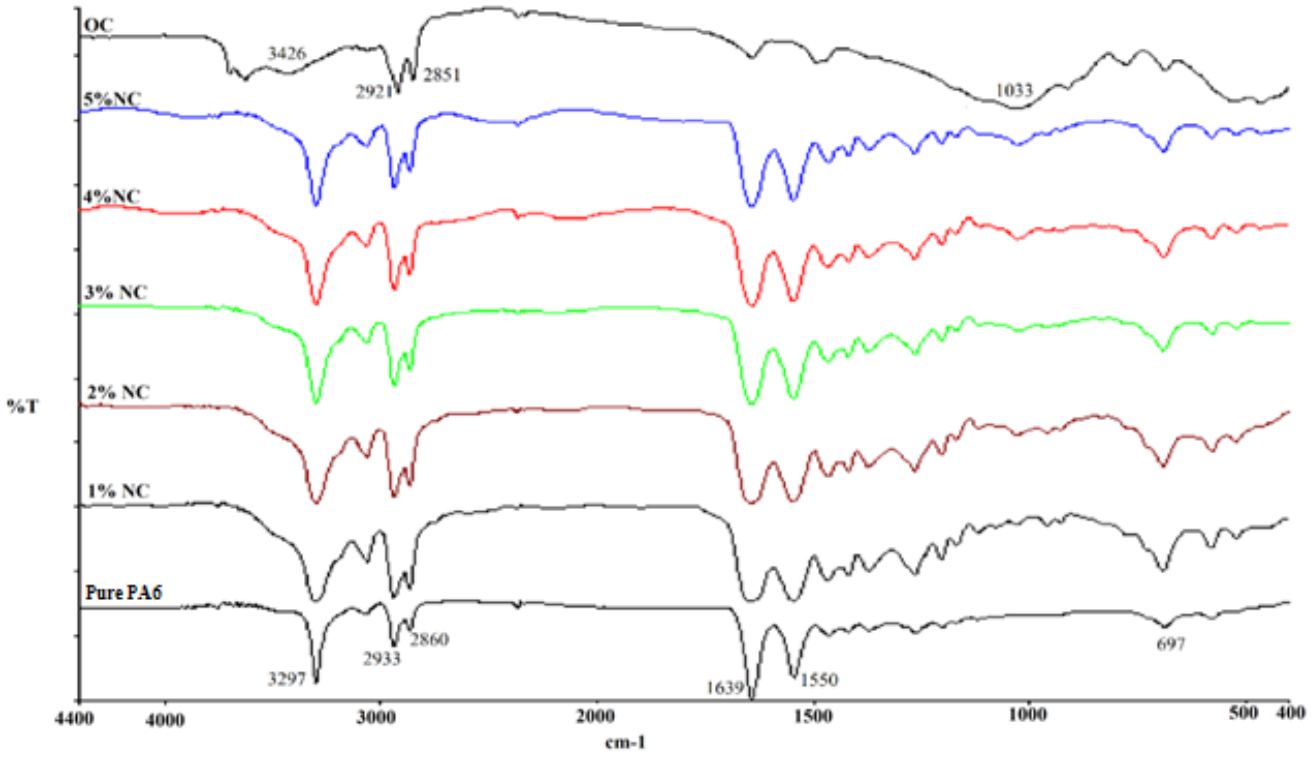

Figure 2. FT-IR spectra of OC, pure PA6 and PA6/OC NCs.

3.1.2 X-Ray Diffraction (XRD)

X-ray diffraction is considered to be a non-destructive and useful technique for identification of the crystalline structure in solid material and analysis of the structural properties of the phases. The distance between the clay layers for raw clay, NaC, OC and the nanocomposite films of PA6/OC were obtained from the peak position of the XRD pattern by using Bragg's equation:

$$2d \sin\theta = n\lambda \qquad (1)$$

where d is the basal distance between the clay layers, λ is the wavelength of the X-ray radiation employed in the experiment (λ= 1.54060 Å), θ is the angle of diffraction beam to the atomic plane and n (equals one here) relates to the order of the reflection. The basal spacing obtained from XRD data give details of the arrangement of surfactant in the OC. In previous studies [21, 22], the monolayer was formed when the d_{001} spacing was about 13.7A°, the bilayer at 17.7A°, the pseudo tri molecular layer at 21.7A° and paraffin complex has a d-spacing larger than 22 A°. **Fig. 3** shows the XRD patterns for RC, NaC and OC. The characteristic peak for RC appeared at 2θ = 6.85 which corresponds to the interlayer distance (d-spacing) of 13.03A°; for NaC, the characteristic peak appeared at 2θ =8.17 which corresponds to the d_{001} spacing of 10.93A°. After the modification of NaC with CPC, the XRD data shows a shift in the characteristic peak position were the d_{001} spacing appeared at 2θ = 4.29 (20.63 A°) for OC. Based on the above data of the d_{001}-spacing of OC, the probable structural configuration of alkyl chain of CPC in the inter lamellar space of clay ranged between the bilayer and pseudo tri molecular layer [21,22].

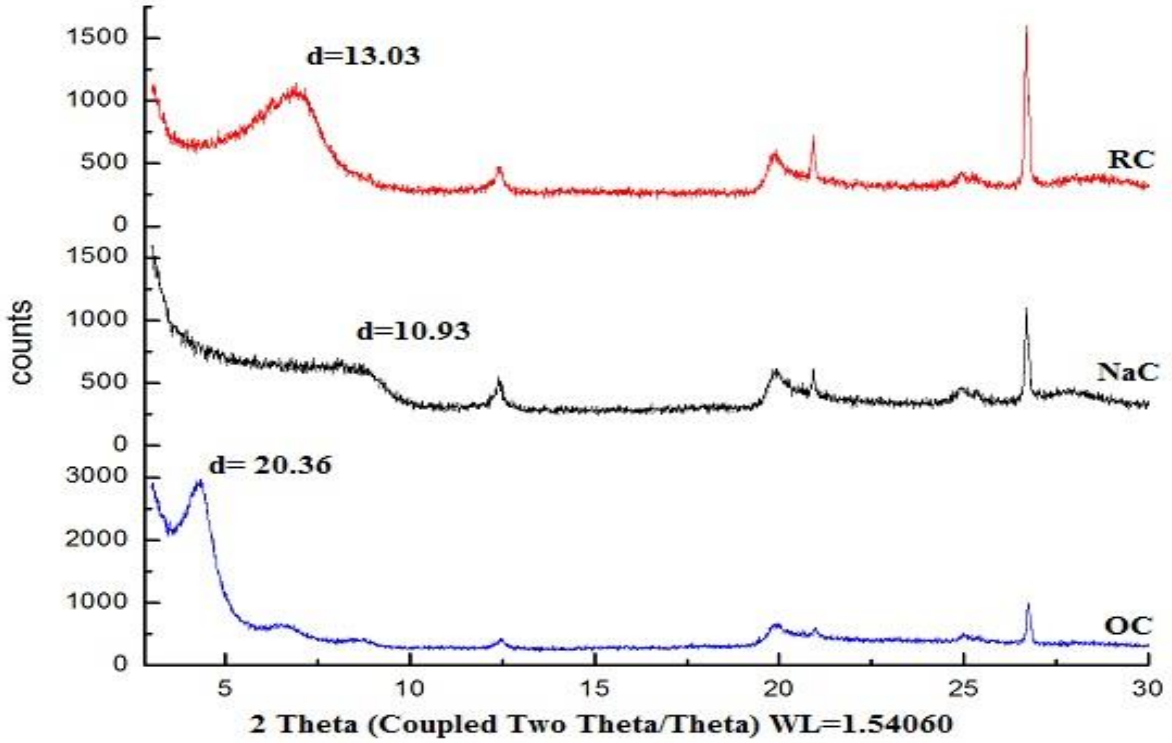

Figure 3. XRD patterns for RC, NaC, OC.

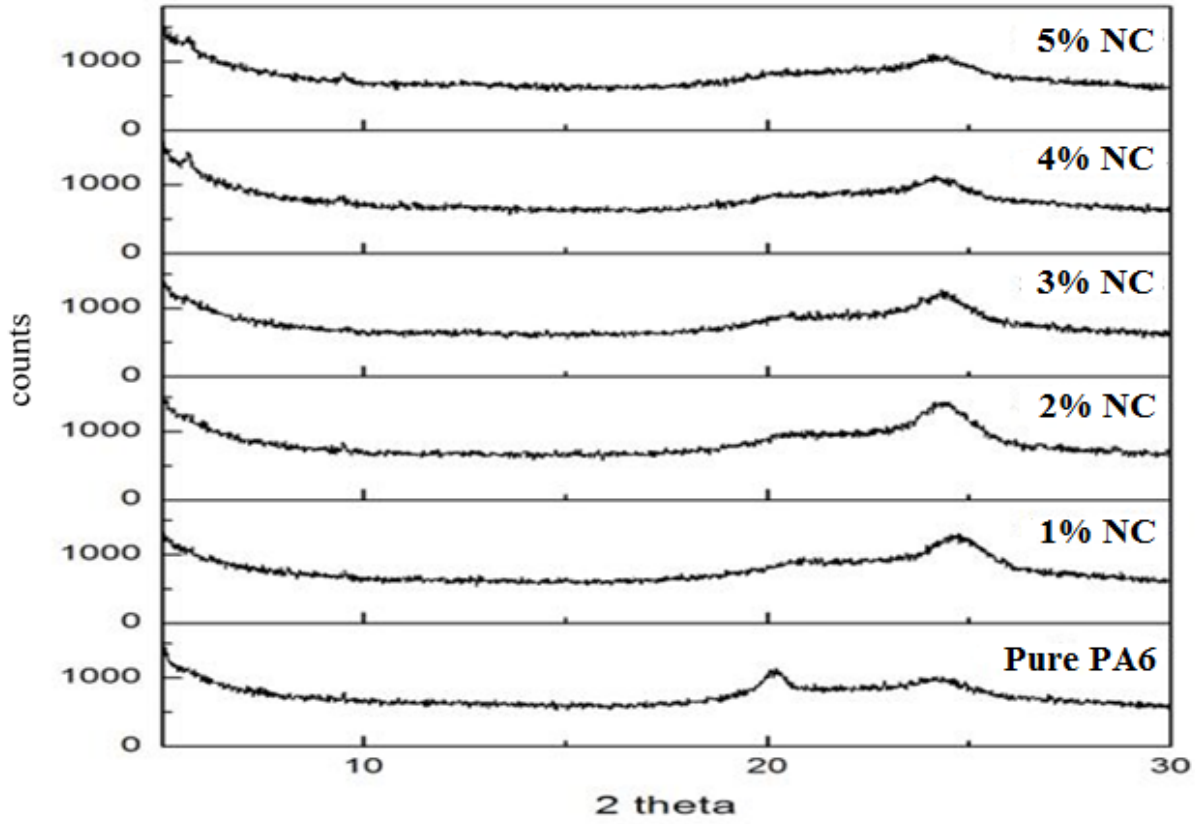

Figure 4. XRD for pure PA6 and PA6/OC NCs.

Fig. 4 shows the XRD patterns for the pure PA6 and PA6/OC NCs that were prepared at different loading of OC (1, 2, 3, 4 and 5wt%). The characteristic peak for RC at 2θ = 4.29 did not appear in 1, 2 and 3% PA6/NCs patterns, which indicates that the OC is well exfoliated in the PA6 matrix. As the OC loading increases to 4 and 5% (PA6/NCs), a diffraction peak with low intensity appeared at 2θ = 3.98 and 2θ = 3.42, respectively. The reduction of these peaks intensity suggested that some of the ordered parallel face–face morphology of silicate layers of OC were disordered [23]. On the other hand, the XRD patterns of pure PA6 in Fig. 4 showed two characteristic peaks at 2θ = 20.2 & 24.35. These peaks are attributed to the crystalline phases, α_1 and α_2, respectively [23]. In the presence of OC, the intensity of α_1 peak was suppressed while the intensity of α_2 peak was increased. These results indicate that the insertion of OC in the PA6 matrix changed the crystallinity behavior of PA [24].

3.1.3. Transmission electron microscopy (TEM)

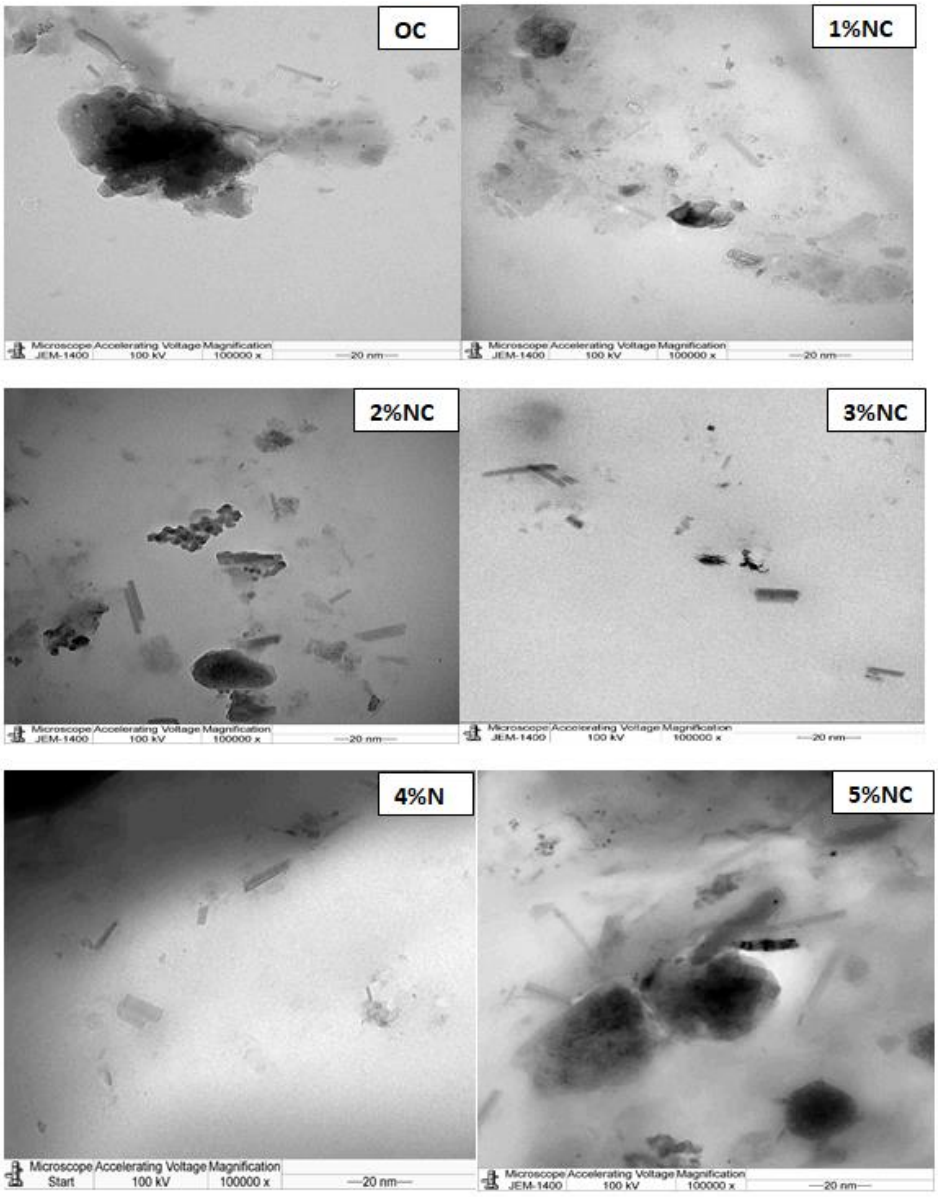

Figure 5A. TEM images of OC and 1-5% NC

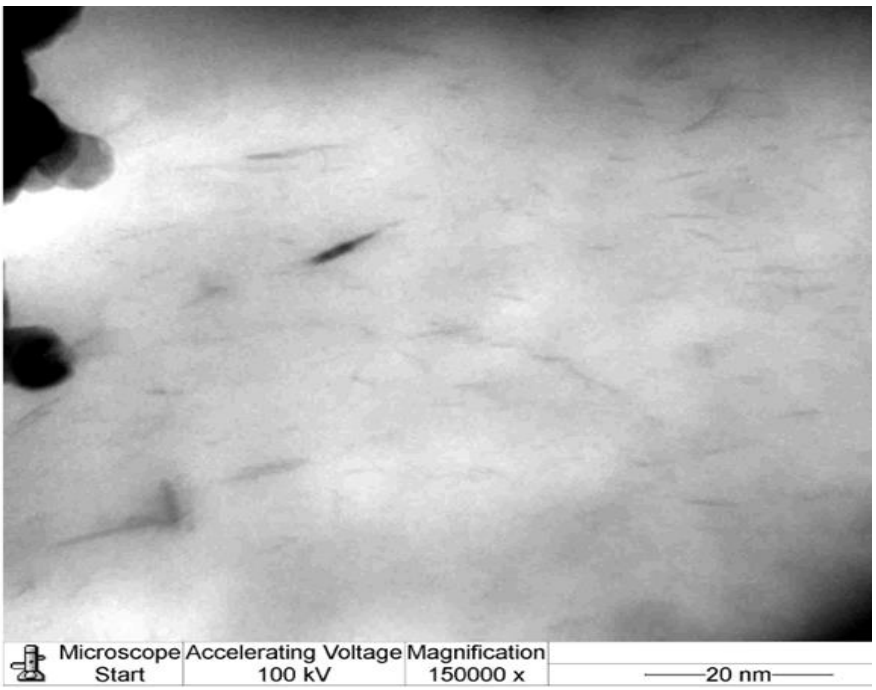

Figure 5B. TEM images of 4 % NC at high magnification

In some cases, XRD measurement can be misleading in determining the level of intercalation and exfoliation in the nanocomposites. The most reliable technique to confirm the presence of exfoliation/intercalation in the nanocomposites is transmission electron microscopy [10]. Fig. 5A represents the OC and PA6/OC NCs. The dark areas represent the OC while the gray/white area represents the PA6 [10]. It is noticed that for PA6/OC NCs with low content of OC (1, 2 and 3% OC), the OC layers were separated and randomly distributed in the polymer matrix which confirm the partially exfoliated structure of the nanocomposite. This observation confirms the XRD result. For 4 and 5% NC with higher OC content, the OC layers are aggregated together which give an indication of the presence of partially exfoliated areas and intercalated structures in small areas. However, when aggregated areas for 4% and 5% were pictured at high magnification, there was countless number of exfoliated structures which look like hair as shown in Fig. 5B which also confirms the XRD data.

3.1.4. Scanning electron microscopy (SEM)

Scanning electron microscopy was used to study the surface morphology of OC, pure PA6 and PA6/OC NCs and to estimate the effect of OC on PA6 structure. Fig. 6 represents SEM images of OC, pure PA6 and Figure 7 represents PA6/OC NCs with different OC loading. In Fig. 6 at 5000 magnification, the surface of pure PA6 looks rough with circular geometric forms. These circular geometric structures consist of spherical agglomerates which confirm the semi crystalline nature of the PA6 [24]. The SEM images of 1, 2, 3 and 5% NC (Fig. 7) show totally different morphology compared to the pure PA6. At high OC loadings, owing to the difference in the scattering density between the clay and PA6, large clay particle aggregates can be easily observed. These particles seem to be easily

deboned and detached from the PA6 matrix due to the poor interfacial adhesion between the OC and PA6 especially at 5%.

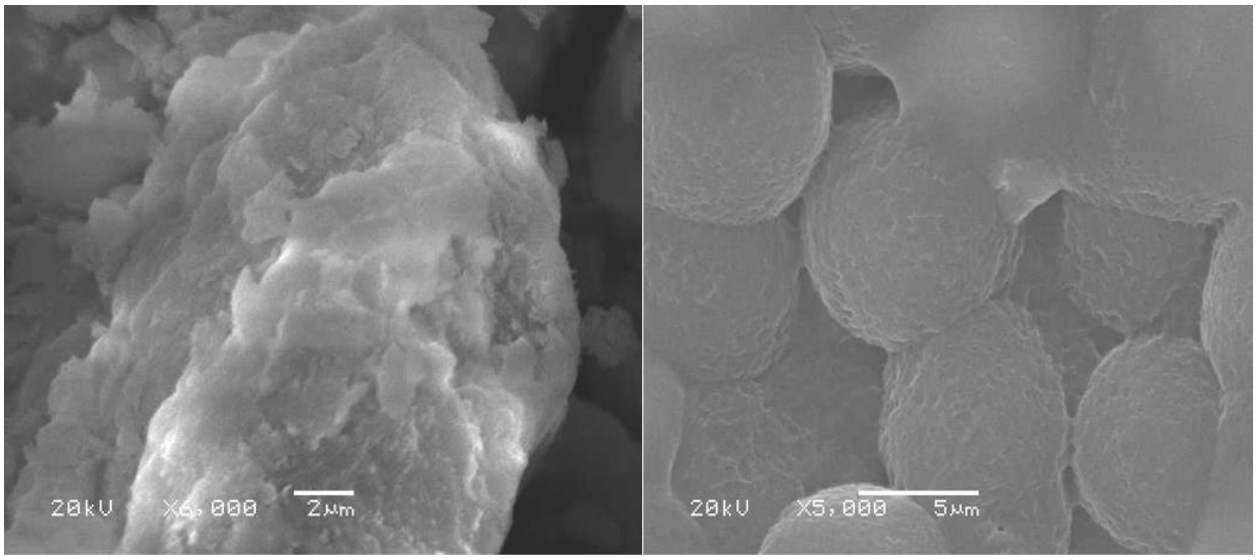

Figure 6. SEM images of OC (left) and pure PA6**.**

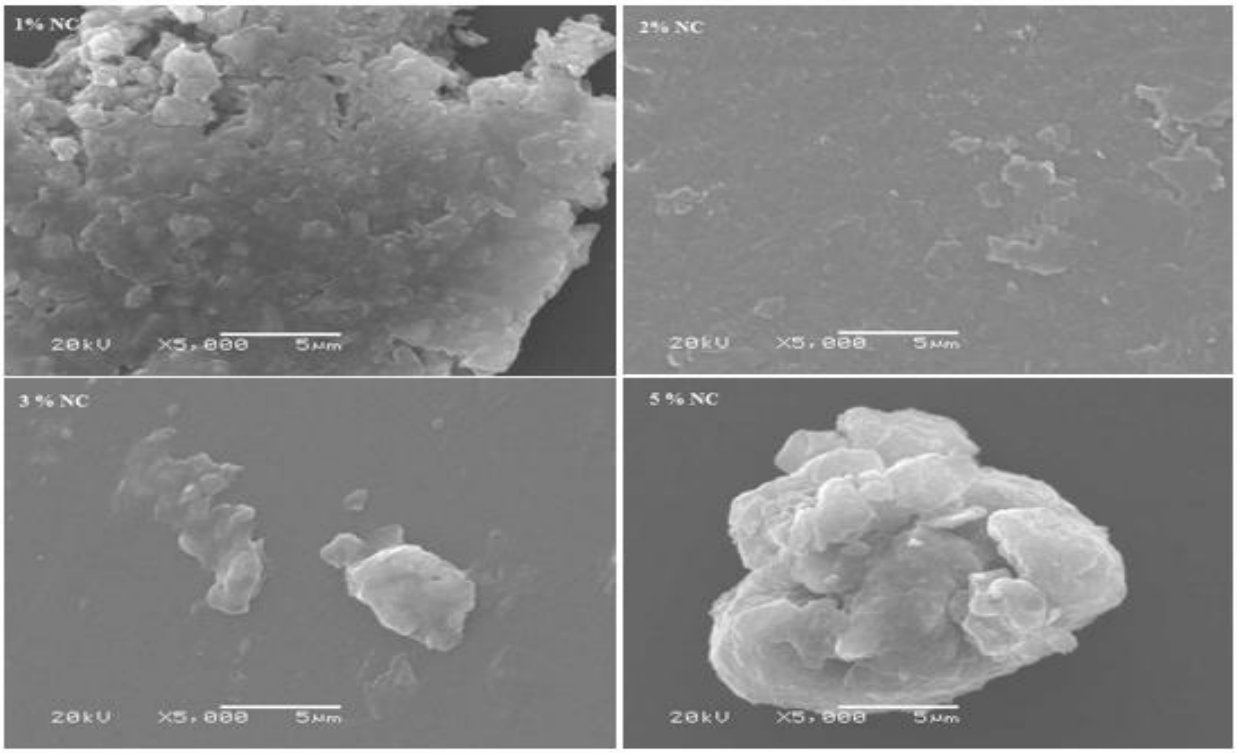

Figure 7. SEM image of PA6/OC NCs with different loading of OC.

3.2. Electrochemical measurements

Three electrochemical techniques were used in this study. We preferred to work on the lower thickness values due to the difficulty of removing the solvent from the prepared PCNs. Thus, a coating thickness of ≈ 15±5 μm was chosen.

3.2.1. Electrochemical impedance spectroscopy (EIS)

The electrochemical impedance spectroscopy (EIS) was an alternative tool to evaluate the corrosion activity variation of C-Steel coated with pure PA6 and PA6/OC nanocomposites.

Five PA6/OC 1,2, 3,4 5% OC loading were chosen to study the electrochemical techniques used in this study. Nyquist plots for the corrosion of C-Steel coated with PA6 and PA6/OC NCs in 3.5% NaCl are shown in Fig. 8. It can be observed that the diameter of the semicircle increases with increase in OC loading. The impedance data were analyzed using an equivalent circuit shown in Figure 9. The circuit consists of the electrolyte solution resistance (R_{sol}), charge transfer resistance (R_c) and double layer capacitance (C_{dl}). The values of R_c and C_{dl} were determined and are listed in Table 1. Clearly, R_c increases, while C_{dl} decreases with the increases in OC loading. A better protection was provided by coating the C-steel with PCN which was accompanied by increasing values of R_c, which can be associated with a slower rate of corrosion. Moreover, a decrease in the values of double layer capacitance of the C-Steel is noticed suggesting that the amount of corrosive molecules reaching the electrode surface decreases as the loading of OC increases [14].

Table 1. EIS parameters for pure PA6 and PA6/OC NCs coating at 30° C in 3.5wt% NaCl, thickness 15 ± 5

Sample	E_{ss} (mV)	R_c (Ohm.cm^2)	C_{dl} (F/cm^2)
Pure PA6	– 373	$1.08 \times 10^{+3}$	0.50×10^{-4}
1% NC	– 253	$1.28 \times 10^{+3}$	1.01×10^{-4}
2% NC	-229	$0.80 \times 10^{+3}$	1.02×10^{-4}
3% NC	– 568	$1.36 \times 10^{+3}$	2.12×10^{-4}
4% NC	-731	$1.24 \times 10^{+3}$	1.82×10^{-4}
5% NC	– 741	$1.42 \times 10^{+3}$	1.80×10^{-4}

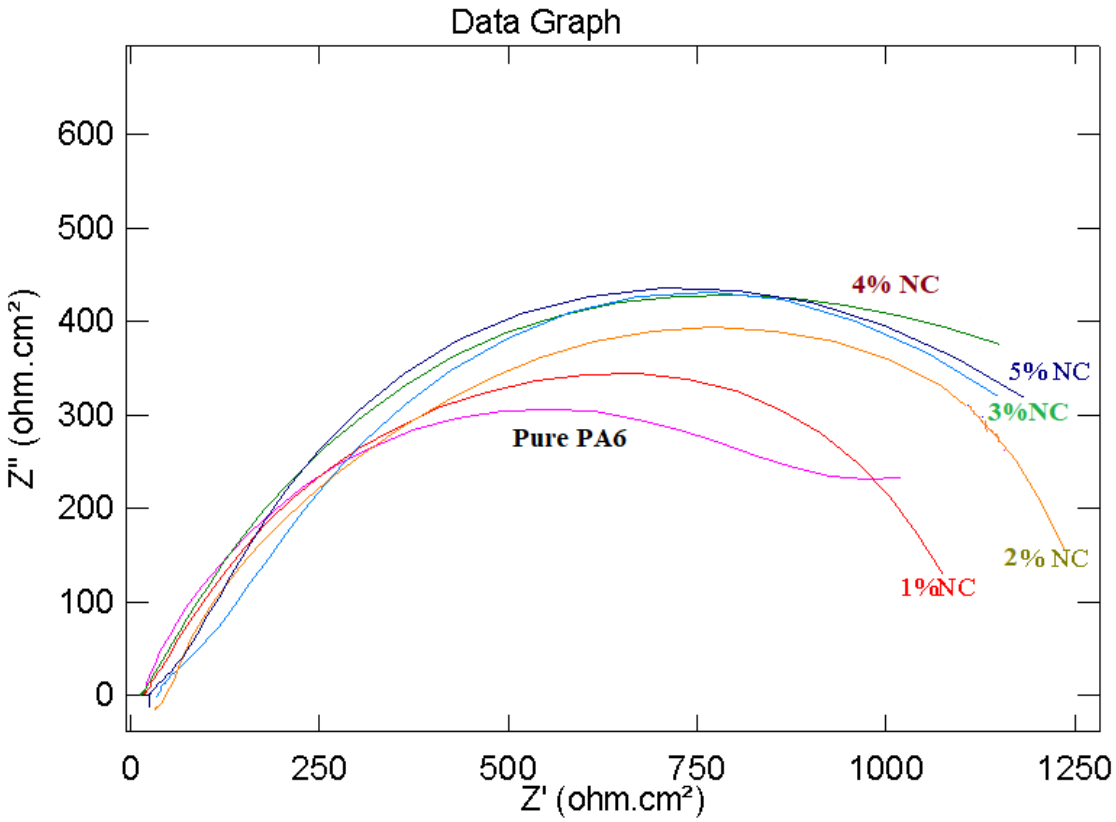

Figure 8. EIS plot for pure PA6 and PA6/OC NCs.

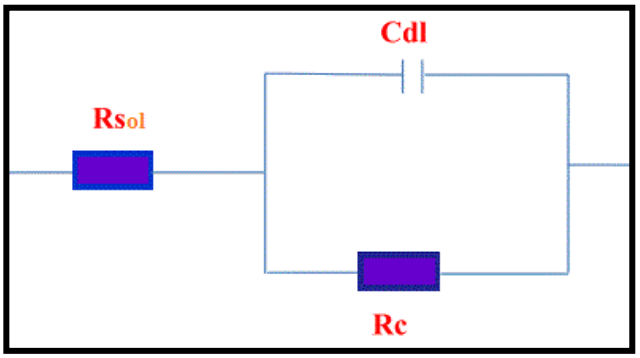

Figure 9. Randle equivalent cell.

3.2.2. Potentiodynamic polarization

Potentiodynamic polarization for pure PA6 and PA6/OC coatings on C-Steel electrodes are recorded after EIS technique in a 3.5% aqueous NaCl electrolyte. Potentiodynamic polarization for PA6, 1,2,3,4, 5% NCs coated C-Steel electrodes are shown in Fig. 10. The corrosion parameters calculated from Potentiodynamic polarization are summarized in Table 2. The anodic and cathodic Tafel constants (B_a and B_c) were determined in volt per current decade from the slope of Tafel lines. Because of the presence of a degree of nonlinearity in the Tafel slopes, the Tafel constants were calculated as a slope of ±30 mV with respect to E_{corr} using a computer least-squares analysis. Corrosion current densities (i_{corr}) and corrosion rates (CR) were determined by the intersection of the cathodic and anodic Tafel lines

at open circuit potential. The percentage of coating or protection efficiency is calculated from the following equation:

$$\% \text{ PE} = \frac{(i\text{corr(PA6)}-i\text{corr(PCN)})}{i\text{corr(PA6)}} \qquad (2)$$

From Table 2, it can be seen that the PA6/OC NCs coated samples show smaller values of i_{corr} than pure PA6 coated samples. Therefore, the incorporation of OC in PA6 matrix, promotes the %PE of PA6/OC NCs coating on C-Steel samples. The anticorrosive efficiency is enhanced as the clay loading is increased. The best corrosion resistance of coated C-Steel was obtained with PA6/OC NCs with 5 wt% of OC where the % Protection efficiency relative to PA6 (%PE) is 75.11%. The enhancement in protection efficiency of PA6/OC NCs compared to pure PA6 coated samples may be attributed to the dispersion and distribution of the silicate layers in the polymer matrix, which increase the tortuosity of diffusion path of the corrosive species such as H_2O and O_2 [25]. In Messersmith and Giannelis study on the barrier properties of PA6-layered silicate nanocomposites, the 4.8% PA6/OC film showed a decrease in permeability compared to pure PA6[26] which is in agreement with our data that 5% NC gave the lowest corrosion rate as shown in Table 1. and Table 2. In a previous work of our research group [15,16], the thickness was 90±5 µm. There was an agreement between electrochemical results and XRD and TEM data when studying the effect of adding 1, 3, 5, 10% of OC to polystyrene to prepare PCN. The lower clay loading (1,3%NC) showed complete exfoliation and the best %PE, then the %PE started to decrease which indicates that there is a critical loading value above which the coating might be affected as described by earlier studies [6,14,15,16]. However, in the present study, we noticed that our electrochemical results are not consistent with results from XRD and TEM techniques where the samples (1-3% NC) which show complete exfoliation from XRD and TEM data did not give the best %PE. On the contrary, the samples of 1-3% NC showed lower %PE compared to 4% and 5%NC.

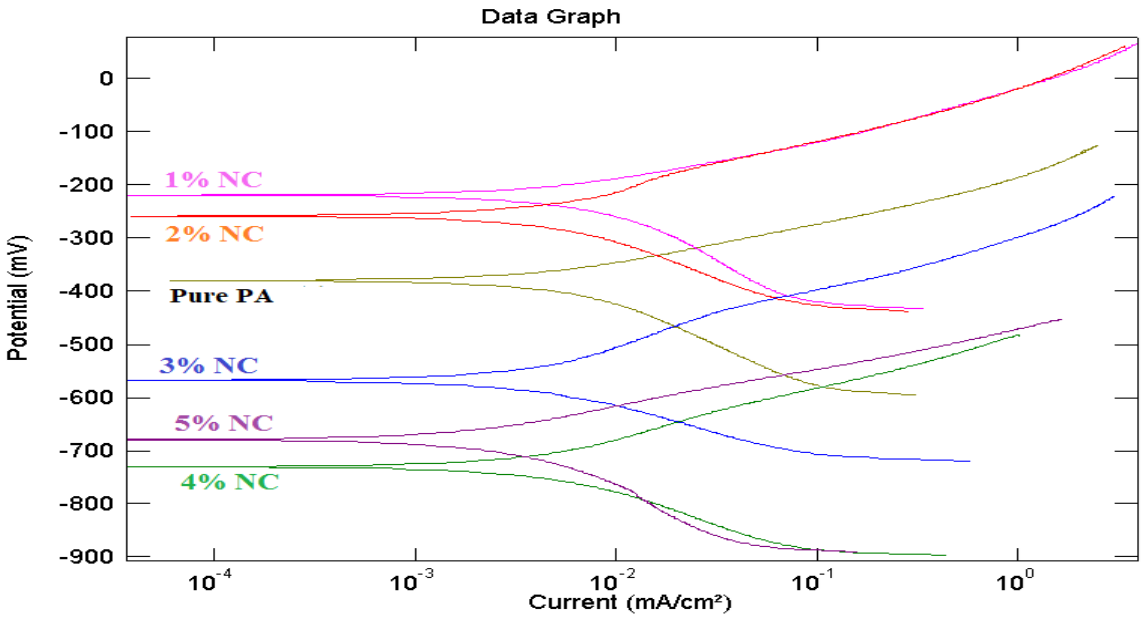

Figure 10. Potentiodynamic polarization graphs for pure PA6 and PA6/OC NCs at 30℃ in 3.5wt% NaCl.

Table 2. Potentiodynamic polarization parameters for PA6 and PA6/OC NC coating at 30° C in 3.5 wt % NaCl, thickness 15 ± 5

Sample	i_{corr} (mA/cm^2)	B_a (mV/dec)	B_c (mV/dec)	CR (mm/year)	%PE
Pure PA6	13.50× 10^{-2}	85	166	1.52	---
1% NC	10.64× 10^{-2}	82	119	1.20	21.10
2% NC	9.85× 10^{-2}	75	95	1.11	26.97
3% NC	8.61× 10^{-2}	80	66	0.97	36.18
4% NC	5.46× 10^{-2}	61	61	0.61	59.87
5% NC	3.35× 10^{-2}	52	48	0.38	75.10

3.2.3. Effect of thickness

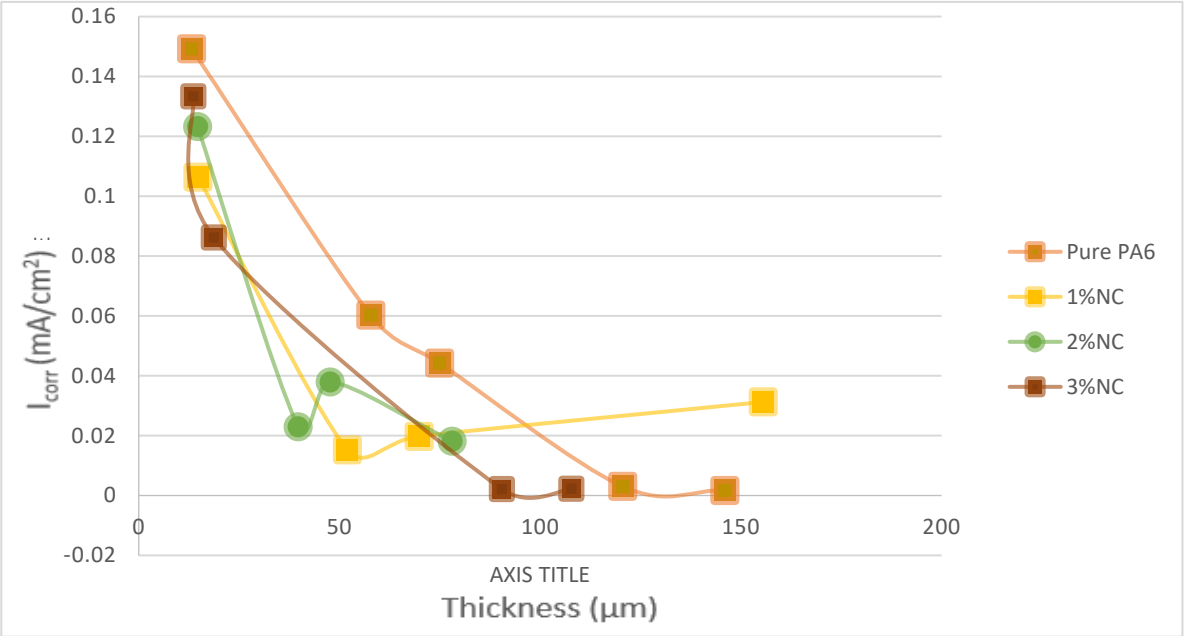

Figure 11. Effect of thickness on i_{corr} for pure PA6 and PA6/OC NCs.

The effect of thickness was studied from Potentiodynamic polarization data. Fig. **11** shows the variation of i_{corr} with coating thickness of PA6 and PA6/OC NCs coating on C-Steel. The coating thickness ranged from 12-140 µm. The i_{corr} value decreased in general with increase in thickness of PA6 and PA6 NCs coating. The coating thickness was chosen based on the ratio (A / d >10^4 cm) where A is the electrode area, d the coating thickness. Mansfield and co-workers have been using an area of 20 cm^2 for coating thickness of 10-50 µm [27].

4. CONCLUSION

Based on the results of XRD, TEM and SEM, the nanocomposites (1, 3 and 5%NC) exhibited corrosion protection performance on C-Steel better than pure PA6. The effective enhancement of anticorrosion properties of PA6/OC NCs, as compared with those of pure PA6 coating, might result from random dispersed silicate nano layers of clay in PA6 matrix that leads to an increase in the tortuosity of the diffusion pathway of the oxygen, water and chloride ions. It could be concluded that the complete dispersion of clay layers in the polymer matrix plays an important role in corrosion resistance. The improvement in the barrier properties formed by polymer/clay nanocomposite can be explained by the concept of tortuous paths, where the permeating molecules are forced to follow a wiggle path around them and diffuse by tortuous pathways especially at high content of OC that leads to an increase in the tortuosity of the diffusion pathway of the oxygen, water and chloride ions. Comparing the R_c and i_{corr} values from this study with our previous study using the same technique of preparing polymer clay nanocomposite using polystyrene instead of PA6 showed that PA6 is not a good polymer to use in preparing polymer clay nanocomposite due to the difficulty in finding a suitable non corrosive solvent. Thus PA6 should not be used in casting solution method but only in melt blending technique like in Toyota research.

ACKNOWLEDGMENTS
This work is from a master thesis of the student Alanood A. Aljaghwani. This research project was supported by a grant from the “Research Center of the Female Scientific and Medical Colleges”, Deanship of Scientific Research, King Saud University.

References

1. Y. Kojima, A. Usuki, M. Kawasumi, A. Okada, T. Kurauchi, O. Kamigaito, *J. Appl. Polym. Sci.*, 49 (1993) 1259.
2. C. P. Bergmann, *Nanostructured Materials for Engineering Applications,* Berlin, Heidelberg: Springer Berlin Heidelberg, 2011.
3. T. D. Fornes, D. R. Paul, Formation and properties of nylon 6 nanocomposites, *Polímeros,* 13 (2003) 212.
4. J.-M. Yeh, S.-J. Liou, C.-G. Lin, Y.-P. Chang, Y.-H. Yu, C.-F. Cheng, *J. Appl. Polym. Sci.,* 92 (2004) 1970.
5. H. Azeredo, L. Mattoso, T. McHugh, *Advances in Diverse Industrial Applications of Nanocomposites*. Intech, Editor Boreddy Reddy, 2011.
6. Abdullah Al-Shahrani, Ihsan Taie, Aziz Fihri and Gasan Alabed, *Polymer-Clay Nanocomposites for Corrosion Protection, Chapter 4* (2018)61.
7. F. Bergaya, B. Theng, G. Lagaley, *Handbook of Clay Science.* Elsevier Publisher, Netherland, 2006.
8. G. Lagaly, *Solid State Ionics,* 22 (1986) 43.
9. D. Chooudalakis, D. Gotsis, *Handbook of Polymer Nanocomposites. Processing, Performance and Application.* Berlin, Heidelberg: Springer Berlin Heidelberg, 2014.
10. C. Powell, G. Beall, Physical properties of polymer/clay nanocomposites, *Curr. Opin. Solid St. M.,* 10 (2006) 73.
11. W. S. Chow, Z. A. Mohd Ishak, *Express Polym. Lett.,* 9 (2015) 211.

12. G. Zehetmeyer, J. M. Scheibel, R. M. D. Soares, D. E. Weibel, M. A. S. Oviedo, R. V. B. Oliveira, *Polym. Bull.,*70 (2013) 2181.
13. B. Ramezanzadeh, S. Niroumandrad, A. Ahmadi, M. Mahdavian, M. H. M. Moghadam, *Corros. Sci.,* 103 (2016) 283.
14. P. Piromruen, S. Kongparakul, P. Prasassarakich, *Prog. Org. Coat.,* 77 (2014) 691.
15. L. A. Al Juhaiman, D. A. Al-Enezi, W. K. Mekhamer, *Digest J. Nanomater. Bios.,* 11 (2016) 105.
16. L. A. Al Juhaiman, *Int. J. Electrochem. Sci.,* 11 (2011) 5618.
17. J. D. Russell, A. R. Fraser, *Infrared methods in Clay Mineralogy: Spectroscopic and Chemical Determinative Methods,* M. J. Wilson, Ed. Dordrecht: Springer Netherlands, 1994, pp. 11–67.
18. L. Qiu, W. Chen, B. Qu, *Polym. Degrad. Stab.,* 87 (2005) 433.
19. R. A. Vaia, H. Ishii, E. P. Giannelis, *Chem. Mater.,*5 (1993) 1694.
20. R. Iwamoto, H. Murase, *J. Polym. Sci. Part B: Polym. Phys.,* 41 (2003) 1722.
21. Y. Xi, Z. Ding, H. He, R. L. Frost, *J. Colloid Interface Sci.,* 277 (2004) 116.
22. Tatiana Munteanu, Claudia Mihaela Ninciuleanu, Ioana Catalina Gifu, Bogdan Trica, ElviraAlexandrescu, Augusta Raluca Gabor, Silviu Preda, Cristian Petcu, Cristina Lavinia Nistor, Sabina Georgiana Nitu and Raluca Ianchis, Intech Open, Chapter 8(2018)147.
23. Y.-H. Yu, J.-M. Yeh, S.-J. Liou, Y.-P. Chang, *Acta Mater.,* 52 (2004) 475.
24. T. D. Fornes, D. R. Paul, *Polymer,* 44 (2003) 3945.
25. P. C. Lebaron, Z. Wang, T. J. Pinnavaia, *Appl. Clay Sci.,* 15 (1999) 11.
26. P. B. Messersmith, E. P. Giannelis, *J. Polym. Sci. Part A: Polym. Chem.,* 33 (1995) 1047.
27. F. Mansfeld, *J. Appl. Electrochem.,* 25 (1995) 187.